Size dependent ion hydration, its asymmetry, and convergence to macroscopic behavior

Sowmianarayanan Rajamani, Tuhin Ghosh, and Shekhar Garde[a)]
The Howard P. Isermann Department of Chemical & Biological Engineering, Rensselaer Polytechnic Institute, Troy, New York 12180

(Received 20 October 2003; accepted 4 December 2003)

The packing and orientation of water molecules in the vicinity of solutes strongly influence the solute hydration thermodynamics in aqueous solutions. Here we study the charge density dependent hydration of a broad range of spherical monovalent ionic solutes (with solute diameters from $\sim$0.4 nm to 1.7 nm) through molecular dynamics simulations in the simple point charge model of water. Consistent with previous experimental and theoretical studies, we observe a distinct asymmetry in the structure and thermodynamics of hydration of ions. In particular, the free energy of hydration of negative ions is more favorable than that of positive ions of the same size. This asymmetry persists over the entire range of solute sizes and cannot be captured by a continuum description of the solvent. The favorable hydration of negative ions arises primarily from the asymmetric charge distribution in the water molecule itself, and is reflected in (i) a small positive electrostatic potential at the center of a neutral solute, and (ii) clear structural (packing and orientation) differences in the hydration shell of positive and negative ions. While the asymmetry arising from the positive potential can be quantified in a straightforward manner, that arising from the structural differences in the fully charged states is difficult to quantify. The structural differences are highest for the small ions and diminish with increasing ion size, converging to hydrophobiclike hydration structure for the largest ions studied here. We discuss semiempirical measures following Latimer, Pitzer, and Slansky [J. Chem. Phys. **7**, 108 (1939)] that account for these structural differences through a shift in the ion radius. We find that these two contributions account completely for the asymmetry of hydration of positive and negative ions over the entire range of ion sizes studied here. We also present preliminary calculations of the dependence of ion hydration asymmetry on the choice of water model that demonstrate its sensitivity to the details of ion–water interactions. [DOI: 10.1063/1.1644536]

I. INTRODUCTION

Many complex biophysical phenomena in aqueous solutions are driven by water-mediated interactions that arise from the peculiar structuring of water near the interacting species. The molecular structure (i.e., packing and orientation) of water near a solute is sensitive to solute–water interactions characterized by the solute geometry and chemistry. Indeed, a variety of phenomena such as salting-in and salting-out of hydrophobic solutes, salt effects on protein stability and solubility, selectivity of ion channels, and the well-known Hofmeister effects, underscore the importance of the charge density dependent hydration of ionic solutes.[1–7]

Differences in the structure of water near ions and their thermodynamic consequences are reflected in the asymmetry of hydration even for the simplest monovalent spherically symmetric ions. In particular, for an ion of a given size, the free energy of hydration of a negative ion is more favorable than that of a positive ion.[8–11] The origin of this asymmetry of hydration lies primarily in the asymmetry of the charge distribution in the water molecule itself, which results in different structural preferences for water molecules near neutral solutes, and positive and negative ions. Clearly, this asymmetry cannot be captured by the Born model which represents water simply as a dielectric continuum with dielectric constant $\epsilon \approx 80$ that gives a symmetric linear response in both positive and negative charging directions. In contrast, molecular simulations represent solvent water molecules explicitly and have the ability to capture the effects arising from the molecular packing and orientation of water molecules near ions. Methodological advances in the treatment of long range interactions in simulations employing periodic boundary conditions[11–15] and systematic studies of system size effects on electrostatic energies have allowed accurate calculations of ion hydration free energies for model monatomic as well as molecular ions.[11,15–17] Spectroscopic experiments on ion–water clusters have also been used previously[18,19] to quantify the thermodynamics of ion hydration. The effect of the nonzero potential of the phase in these experiments on ion–water clusters has been discussed in detail by Asthagiri *et al.*[20] But, simulations of ion hydration in bulk solution that use conducting "*tin-foil*" boundary conditions, enforce a zero reference potential and hence the calculated free energies of hydration are absolute.

The surface of a typical biomolecular solute is complex, and presents a nonhomogeneous distribution of charge den-

a)Author to whom correspondence should be addressed. Electronic mail: gardes@rpi.edu

TABLE I. Lennard-Jones parameters for ion–water interactions (Refs. 64–66). Larger ions are named by their σ_{i-O} values, as in 0.6, 0.8, 1.0 in nm units. Ion (σ_{i-i} and ϵ_{i-i}) and water (σ_{O-O} and ϵ_{O-O}) LJ parameters are combined using Lorentz–Berthelot rules: $\sigma_{i-O}=0.5(\sigma_{i-i}+\sigma_{O-O})$ and $\epsilon_{i-O}=(\epsilon_{i-i}\epsilon_{O-O})^{1/2}$.

Ions	σ_{i-O}, nm	ϵ_{i-O}, kJ/mol	Ions	σ_{i-O}, nm	ϵ_{i-O}, kJ/mol
Li	0.2337	0.6700	Cl	0.3785	0.5216
Na	0.2876	0.5216	Br	0.3896	0.5216
K	0.3250	0.5216	I	0.4168	0.5216
Rb	0.3348	0.5216	0.6	0.6000	0.5216
Cs	0.3526	0.5216	0.8	0.8000	0.5216
F	0.3143	0.6993	1.0	1.0000	0.5216

sities leading to local solvation patterns ranging from ionic (with high positive or negative charge densities) to hydrophobiclike (with low or zero charge densities) hydration. The hydration phenomena in such complex solutes may be understood through simulations of simple spherically symmetric model solutes over a range of charge densities or solute sizes. For small ions, the asymmetry of hydration arising from different packing and orientational preferences of water molecules near negative and positive ions is well known. That asymmetry is expected to diminish with increasing solute size, leading to the convergence of hydration behavior in the large solute limit. This was studied recently by Ashbaugh through calculations of the hydration free energies of hard-sphere ions as a function of ion size.[21] Ashbaugh found that although the hydration asymmetry diminishes with increasing ion size, it does not vanish completely for the largest ions. It was argued that the inherent structural preferences of water near neutral solutes lead to a small positive potential at the solute center,[11,21–23] and therefore, bias the charging process in the negative direction favorably. Upon accounting for this bias, he obtained convergence of the hydration free energies of large negative and positive ions. Ashbaugh's study raises several important questions with regards to ion hydration structure and thermodynamics. For example, for hydrophobic solutes with radii larger than about ~ 3.5 Å, the density of water in contact with solutes drops monotonically with increasing solute size.[24–26] For solutes with attractive solute-water interactions, Hummer and Garde characterized this phenomenon[24] as a weak dewetting of the solute surface. Do ionic solutes dewet similarly with increasing solute size? How sensitive are the orientational preferences of vicinal water molecules to the ion size? Specifically, to account for the hydration asymmetry over the entire range of ion sizes it will be important to quantify systematically both packing and orientational differences of water near positive and negative ions and their dependence on the ion size

Here we use molecular dynamics simulations of spherical monovalent ions in $0e$, $-1e$, and $+1e$ charge states to calculate their free energy of charging. A wide range of ion sizes from small ions ($r_{ion}\sim 0.2$ nm) that exhibit the highest asymmetry to relatively large ions ($r_{ion}\sim 0.85$ nm) that show near symmetric hydration behavior with respect to charging are studied. We specifically focus on the structural (packing and orientational) properties of hydration water, to monitor the convergence of positive and negative ion hydration to macroscopic continuum behavior. We systematically identify the molecular origins of ion hydration asymmetry and quantify their relative contributions. Ion hydration thermodynamics and structure obtained from molecular simulations will clearly depend on the water model used. To this end, we present preliminary calculations of the hydration of a fluoride ion in four different models of water (SPC, SPC/E, TIP3P, and TIP4P). Collectively, our results provide a clearer picture of ion hydration structure and thermodynamics as a function of ion size.

II. METHODS

A. Details of molecular dynamics simulations

Molecular dynamics simulations of single ions in a cubic box of water molecules were carried out at constant temperature of 300 K and a pressure of 1 atm using GROMACS.[27,28] Ions were represented as Lennard-Jones solutes with the charge placed at their center. The simple point charge (SPC) model[29] was used to represent water molecules explicitly. Ion–water interaction parameters for 12 different ions are listed in Table I. We do not include the polarizability of ions or water molecules in our calculations. Previous calculations have shown that the free energy of hydration of ions is relatively insensitive to the inclusion of polarizability in the models for ions and water molecules.[30,31] The effects of polarizability may become appreciable in interfacial[32,33] or ion–water cluster systems, but such systems are not the focus of this work.

A separate simulation of each of the 12 ions was performed in three different charge states, $+1e$, $0e$, and $-1e$, where e is the electronic charge. The range of ion sizes from lithium ion to the largest ion with $\sigma_{ion-water}$ (or σ_{i-O}) $=1$ nm in negative, neutral, and positive charge states allows us to study systematically the effect of ion size and charge on the hydration structure and thermodynamics. For ions with σ_{i-O} smaller than 0.6 nm, 128 water molecules were included in the simulation, whereas for the three larger ions, significantly larger number of water molecules *viz.* 1405, 2472, and 4000 were included. System size corrections to electrostatic energies were applied as discussed in Refs. 14–17. Simulations of a fluoride ion were carried out in neutral, positive, and negative charge states in four different water models simple point charge,[29] simple point charge-extended (SPC/E),[34] transferable intermolecular potential three-point (TIP3P), and four-point (TIP4P)[35] to assess the effect of water model on the hydration free energy.

Periodic boundary conditions were applied and particle mesh Ewald method[36] was used to calculate the electrostatic

interactions with a grid spacing of 1 Å. A time step of 2 fs was used in all simulations. Nose–Hoover[37,38] and Parrinello–Rahman[39,40] algorithms were used to maintain the systems at a constant temperature and pressure. The coupling times for the thermostat and the barostat were 0.1 ps and 0.5 ps, respectively. For large solutes, the solvent and the solute were separately coupled to the thermostat with the same time constant for coupling of 0.1 ps. The SETTLE algorithm[41] was used to constrain OH and HH distances in water with a geometric tolerance of 0.0001 Å. Equilibration runs were carried out for 1 ns followed by production runs of 4–6 ns amounting to a total simulation time of 210 ns. Configurations were saved every picosecond for analysis.

B. Calculation of the free energy of charging

The hydration free energy of an ion can be calculated by summing the free energy of hydration of a neutral solute and the free energy of charging that neutral solute to the fully charged state. Both of these terms can be calculated using the ideas from perturbation theory as discussed in detail elsewhere.[11,15,42,43] Free energy of transfer of a neutral hydrophobic solute from an ideal gas state to water has been extensively studied previously.[44–47] This term does not contribute to the asymmetry of ion hydration free energy. Below, we focus only on the calculation of the charging free energy. Details of the calculation of the free energy of ion charging have been discussed thoroughly elsewhere.[11,13,16,17,22] Here we present only the necessary equations and refer the reader to those Refs. 11, 13, 17, and 42 for further details. The free energy of ion charging can be written as

$$\Delta\mu^{ex} = -kT \ln\langle \exp(-\beta\Delta u)\rangle_{\lambda_0}, \tag{1}$$

where $\beta = 1/kT$, k is the Boltzmann constant, T is the temperature, λ is a charging parameter, and the subscript λ_0 indicates the initial charge state over which the ensemble average is calculated. For the charging process, $\lambda = 0$ corresponds to the neutral state ($q = 0$) and $\lambda = 1$ to the fully charged state ($q = \lambda q_{\text{ion}} = +e$ for positive and $-e$ for negative monovalent ions, where e is the electronic charge). The difference in energy, $\Delta u(\lambda_0 \rightarrow \lambda_1)$, between the charge states λ_1 and λ_0 of the ion, results from changes in ion–water electrostatic energy and the self-energy of the ion,

$$\Delta u = q_{\text{ion}}(\lambda_1 - \lambda_0)\phi + (\lambda_1^2 - \lambda_0^2)u_s, \tag{2}$$

where ϕ is the instantaneous electrostatic potential due to the surrounding medium at the center of the ion in charge state λ_0; and u_s (in kJ/mol) $= -2.837\,297 e^2/L$, is the self-energy of the ion in the fully charged state ($q = q_{\text{ion}}$), where L is length of the cubic periodic box in nm. Substituting for Δu in Eq. (1), we get

$$\Delta\mu^{ex} = -kT \ln\langle \exp[-\beta q_{\text{ion}}(\lambda_1 - \lambda_0)\phi]\rangle_{\lambda_0} + (\lambda_1^2 - \lambda_0^2)u_s. \tag{3}$$

The resulting cumulant expansion[11,17] of Eq. (3) about the state λ_0 gives

$$-\beta\Delta\mu^{ex} = \sum_{n=1}^{\infty} \frac{(-\beta q_{\text{ion}}\Delta\lambda)^n}{n!} C'_{n,\lambda_0}, \tag{4}$$

where $\Delta\lambda = \lambda_1 - \lambda_0$, and the cumulants C'_{n,λ_0} quantify the fluctuations in electrostatic energy in state λ_0. The prime indicates that the values of cumulants are corrected by applying system size corrections as discussed in detail previously.[11,14,17,43] Thus,

$$C'_{1,\lambda} = \langle\phi\rangle_\lambda + 2\lambda u_s/q_{\text{ion}}, \tag{5}$$

$$C'_{2,\lambda} = \langle(\phi - \langle\phi\rangle_\lambda)^2\rangle_\lambda - 2kTu_s/q_{\text{ion}}^2. \tag{6}$$

The third and higher order cumulants do not require system size corrections and are related to the higher order moments of probability distribution of the electrostatic potential ϕ. Equation (4) essentially represents a Taylor series expansion of the free energy of charging, and therefore, the cumulants can be related to derivatives of free energy with respect to charge on the solute, $q = \lambda q_{\text{ion}}$. That is,

$$\left[\frac{\partial^n \Delta\mu^{ex}}{\partial q^n}\right] = (-\beta)^{(n-1)} C'_{n,\lambda}, \quad n \geqslant 1. \tag{7}$$

We used the Ewald summation method to evaluate the cumulants (see Ref. 17 for details). Hummer and Szabo[43] have derived expressions for combining information about free energy derivatives from simulations of initial and final states to best estimate free energy differences. We calculated the first and second cumulants for neutral as well as fully charged states of ions and used the following expression to calculate the free energy of charging ΔG:

$$\Delta G \approx \frac{q_{\text{ion}}}{2}(C'_{1,\lambda=0} + C'_{1,\lambda=1}) - \frac{\beta q_{\text{ion}}^2}{12}(C'_{2,\lambda=0} - C'_{2,\lambda=1}), \tag{8}$$

which is exact to the fourth order of free energy perturbation theory.

III. RESULTS AND DISCUSSION

A. Free energy of charging of ions

Table II lists cumulants (i.e., derivatives of free energy with respect to the ion charge) for all ions in their neutral ($\lambda = 0$) and fully charged ($\lambda = 1$) states. Calculations of cumulants for ion hydration have been performed previously and their features have been thoroughly discussed.[11,17,48] The first cumulant, $C'_{1,\lambda}$, gives essentially the average value of electrostatic potential at the ion center in the charge state λ, whereas the second cumulant, $C'_{2,\lambda}$, provides information about the fluctuations of the electrostatic potential at the ion center (i.e., the width of the probability distribution of the electrostatic potential). The electrostatic potential at the center of the ion is induced primarily by the orientational polarization of water molecules in the vicinity of the ion while thermal fluctuations in the position and orientation of those water molecules lead to fluctuations in the electrostatic potential at the ion center.

Table II also lists values of free energies, ΔG [using Eq. (8)], of charging the ion from neutral to fully charged states for various positive and negative ions. ΔG values are negative, as expected, and decrease in magnitude with increasing ion size. Figure 1 compares the free energies of charging as a function of ion radius ($r_{\text{ion}} = \sigma_{\text{ion–ion}}/2 = \sigma_{i-\text{O}} - \sigma_{\text{O–O}}/2$)

TABLE II. Free energy of charging of ions from neutral to $-1e$ and $+1e$ charge states. First and second cumulants corrected for system size, in the charged and uncharged states, $C'_{1,\lambda}$ and $C'_{2,\lambda}$, are also reported. Numbers enclosed in parentheses are error bars. All quantities are in kJ/mol.

Ion	$C'_{1,\lambda=0}$	$\beta C'_{2,\lambda=0}$	$C'_{1,\lambda=1}$	$\beta C'_{2,\lambda=1}$	ΔG
Li^+	43.0(1.4)	1088.1(71.2)	−956.3(1.5)	806.3(24.2)	−480.2(9.4)
Na^+	38.6(1.6)	774.8(39.6)	−780.2(2.8)	887.1(34.9)	−361.5(8.4)
F^+	36.8(1.1)	673.3(24.3)	−652.3(2.5)	808.9(21.8)	−296.3(5.6)
K^+	35.3(1.5)	695.6(25.0)	−640.7(2.0)	759.7(36.1)	−297.3(6.8)
Rb^+	36.5(1.5)	645.5(23.1)	−610.1(1.7)	739.1(42.6)	−279.0(7.1)
Cs^+	34.8(0.9)	588.7(18.8)	−561.7(1.1)	680.9(42.5)	−255.4(6.1)
Cl^+	35.4(1.5)	539.4(14.0)	−504.5(1.7)	597.1(21.4)	−229.7(4.5)
Br^+	35.4(1.0)	536.9(16.0)	−482.5(1.0)	582.3(20.9)	−219.7(4.1)
I^+	34.2(0.8)	523.6(18.8)	−438.0(1.3)	512.7(9.0)	−202.8(3.4)
0.6^+	36.7(1.3)	315.1(10.9)	−262.9(1.0)	301.2(13.4)	−114.3(3.2)
0.8^+	38.1(2.3)	229.5(20.8)	−181.9(1.2)	218.8(5.8)	−72.8(4.0)
1.0^+	39.2(1.7)	173.9(7.4)	−133.7(1.5)	191.1(24.4)	−45.7(4.2)
Na^-	38.6(1.6)	774.8(39.6)	1342.7(2.4)	1060.7(52.8)	−666.8(9.7)
F^-	36.8(1.1)	673.3(24.3)	1059.1(1.9)	972.8(69.3)	−523.4(8.8)
K^-	35.3(1.5)	695.6(25.0)	1034.5(2.1)	977.4(59.0)	−511.5(8.8)
Cs^-	34.8(0.9)	588.7(18.8)	886.7(1.5)	890.7(42.3)	−435.6(6.3)
Cl^-	35.4(1.5)	539.4(14.0)	773.5(1.7)	808.3(28.2)	−382.0(5.1)
Br^-	35.4(1.0)	536.9(16.0)	739.3(1.0)	737.2(30.2)	−370.7(4.8)
I^-	34.2(0.8)	523.6(18.8)	650.5(1.9)	674.9(29.2)	−329.7(5.4)
0.6^-	36.7(1.3)	315.1(10.9)	376.2(1.4)	370.1(14.0)	−204.3(4.0)
0.8^-	38.1(2.3)	229.5(20.8)	272.4(1.7)	230.1(23.8)	−155.2(5.7)
1.0^-	39.2(1.7)	173.9(7.4)	219.2(1.7)	182.8(7.8)	−128.6(2.9)

(Ref. 68) obtained from MD simulations, with the predictions of the Born model. Although the variation in values calculated from MD simulations is similar to that predicted by the Born equation, ΔG values for positive (negative) ions are unfavorable (favorable) with respect to the continuum model predictions.

Hummer *et al.*[11] as well as Ashbaugh[21] have discussed the origins of the hydration asymmetry with respect to the charging direction. This asymmetry arises partly from the water structural arrangements near neutral solutes that lead to a small positive electrostatic potential, $\langle\phi\rangle_0$, at the center of the neutral solute. Thus, charging in the negative direction is more favorable compared to that in the positive direction. The inset of Fig. 1 shows the values of $\langle\phi\rangle_0$ (i.e., the first cumulant in the uncharged state, in kJ/mol), calculated from MD simulations as a function of solute size. These values are in excellent agreement with those reported by Ashbaugh.[21] $\langle\phi\rangle_0$ is positive for the smallest ions ($\sim$43 kJ/mol), decreases slightly with increasing ion size before increasing again smoothly to its asymptotic value of approximately 40 kJ/mol. For small hydrophobic solutes, water molecules in the vicinity straddle the solute surface with their HOH planes lying almost parallel to the solute surface. In these orientations, water hydrogens are slightly closer to the solute center compared to oxygens leading to the net positive electrostatic potential at the solute center. Water molecules near large solutes and flat surfaces are also oriented predominately parallel to the surface with some bias toward pointing one of the hydrogens directly to the surface[21,47,49–54] resulting in a slightly positive electrostatic potential on the solute side of the interface.

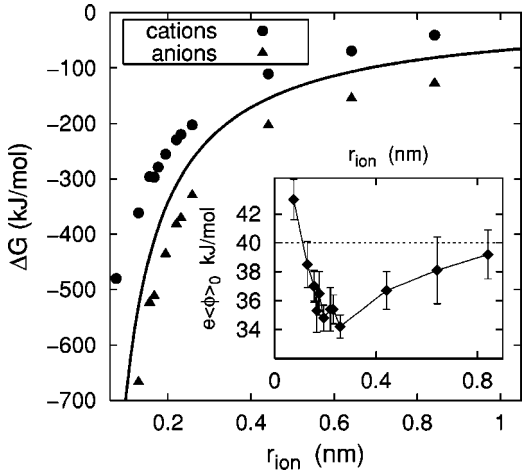

FIG. 1. Free energy of charging of LJ ions as a function of ion radius ($r_{\text{ion}}=\sigma_{i-i}/2$) calculated from molecular dynamics simulations (symbols). ΔG values predicted using Born equation [$\Delta G=-(q^2/2r_{\text{ion}})(1-1/\epsilon)$, where $\epsilon\sim65$ for SPC water (Ref. 67)] is shown by the solid line. The inset shows the average electrostatic potential, $e\langle\phi\rangle_0$, at the center of an uncharged solute as a function of solute size.

The limiting value of $\langle\phi\rangle_0$ calculated here for larger solutes compares well with that reported previously for the SPC water-vapor interface.[53] However, as pointed out earlier by Pratt[50] and Sokhan and Tildesley,[52] the exact numerical value of the electrostatic potential is sensitive to the model of water simulated. Experimental estimates of the surface potential across a water–vapor interface also differ widely both in terms of its sign and magnitude.[55] Thus, quantitative comparisons of our results on the limiting value of $\langle\phi\rangle_0$ with experimental data is not possible. Nevertheless, without loss of consistency, the positive potential is seen to contribute significantly to the asymmetry of the charging free energy in

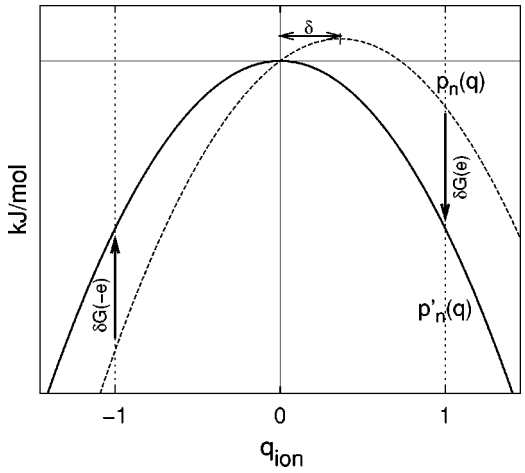

FIG. 2. A schematic illustrating asymmetry in the hydration free energy, resulting from the positive potential at the center of a neutral solute. The dashed curve shows $p_n(q)$, an nth order fit to the free energy of charging, using information from the charged as well as the uncharged states. To make the curve symmetric, the vertex of the polynomial fit is shifted to the origin; the resultant plot is shown as the solid line ($p'_n(q)$).

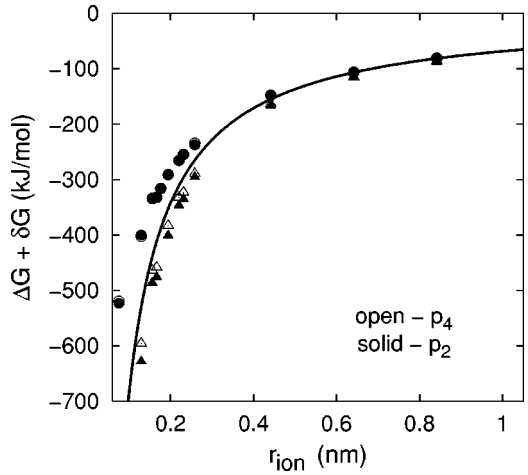

FIG. 3. Modified free energy of charging of cations (circles) and anions (triangles) calculated using the scheme of Fig. 2 using p_2 [Eqs. (9) and (10)] and p_4 [Eqs. (11) and (13)] approximations for ΔG. Solid line shows the Born prediction. δG accounts for the asymmetry arising from the positive potential at the center of a neutral solute. The asymmetry in hydration persists for smaller ions and disappears only for ions of radii 0.5 nm or more.

our calculations. We defer the discussion on the water model dependence of $\langle\phi\rangle_0$ to Sec. III D.

Ashbaugh showed that when the contribution from the positive potential at the center of neutral solute, $q_{\text{ion}}\langle\phi\rangle_0$, is subtracted from ΔG, the modified free energy (Ref. 69) as a function of ionic charge becomes symmetric for large ions ($r_{ion}>5$ Å). We explore the origin of this contribution mathematically and provide further improvement and insights. The cumulant expansion [Eq. (4)] constitutes an expansion of the free energy of charging in the powers of ionic charge about a given charge state. The simplest reasonable approximation for the free energy of charging about the $q=0$ state is obtained by truncating the expansion at the quadratic level. Thus,

$$\Delta G(0\rightarrow q)=p_2(q)=a_1q+a_2q^2, \tag{9}$$

where $a_1=C'_{1,0}$ and $a_2=-\beta C'_{2,0}/2$. The slope of this parabola at $q=0$, equal to $\langle\phi\rangle_0$, is positive and the vertex of the parabola is located at $q=\delta$ as shown in Fig. 2. In contrast, the Born model predicts a quadratic dependence of free energy on charge ($\Delta G\propto q^2$) with a slope of 0 at $q=0$. The asymmetry in the calculated free energies of hydration resulting from the positive potential at the center of an uncharged solute can be accounted for by translating the parabola vertically and horizontally such that it has a zero slope at the origin (see Fig. 2). The translated parabola $p'_2(q)$ is obtained as

$$p'_2(q)=p_2(q+\delta)-p_2(\delta). \tag{10}$$

Interestingly, the shift $p'_2(q)-p_2(q)$ is equal to $-q_{\text{ion}}\langle\phi\rangle_0$, identical to the shift used by Ashbaugh.[21] The free energy of charging, although quadratic with charge in each direction, has a larger curvature in the negative direction as compared to that in the positive direction.[11,56] When more information about cumulants is available in different charge states, as is the case here, higher order polynomials can be used instead of a quadratic to represent the free energy of charging more accurately and to capture the asymmetry in hydration better.[17,43] For example, using the first and second order cumulants in neutral and fully charged states, we obtain an exact fourth order polynomial fit for ΔG,

$$\Delta G(0\rightarrow q)=p_4(q)=a_1q+a_2q^2+a_3q^3+a_4q^4, \tag{11}$$

where

$$a_1=C'_{1,0},$$

$$a_2=\frac{-\beta C'_{2,0}}{2},$$

$$a_4=\frac{-\beta(C'_{2,0}+C'_{2,1})+2(C'_{1,0}-C'_{1,1})}{4},$$

$$a_3=\frac{-\beta(C'_{2,1}-C'_{2,0})-12a_4}{6} \quad \text{for } q=+1,$$

$$a_3=\frac{\beta(C'_{2,1}-C'_{2,0})+12a_4}{6} \quad \text{for } q=-1. \tag{12}$$

For each solute, we fit independent fourth order polynomials for both positive and negative charging directions. The maximum of each $p_4(q)$ curve can be translated to the origin as before *viz.*,

$$p'_4(q)=p_4(q+\delta)-p_4(\delta). \tag{13}$$

The two translated quartics combine to give a composite ΔG vs q curve, the resultant curve has a slope of 0 at $q=0$ and is continuous and differentiable over the entire range $[-1,1]$. The corresponding shift in the free energy of charging, δG, is given by $p'_4(q)-p_4(q)$.

Figure 3 shows the modified free energy of charging, $\Delta G+\delta G$, where δG is approximated using the p_2 fit [Eqs. (9) and (10)] and the p_4 fit [Eqs. (11) and (13)] for ΔG. We observe that the shift obtained using p_4 is nearly identical to that obtained using p_2 for all positive ions and large negative

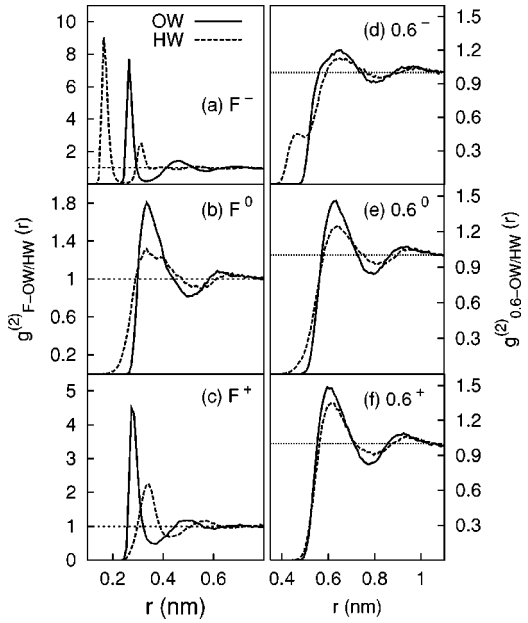

FIG. 4. Ion–oxygen (solid line) and ion–hydrogen (dashed line) rdfs for fluoride and 0.6 nm ions in three different charge states: (a) F^-, (b) F^0, (c) F^+, (d) 0.6^-, (e) 0.6^0, (f) 0.6^+.

ions but differs for the smallest negative ions. As observed earlier,[21] the modification obtained using the quadratic fit, $q_{\text{ion}}\langle\phi\rangle_0$, constitutes a significant part of the asymmetry. Indeed, as seen in Fig. 3, the ΔG values modified using the quadratic fit appear to converge to the values predicted by the Born model for larger ions ($r_{\text{ion}} \geqslant 5$ Å).

A significant asymmetry persists however for smaller ions, with negative ions being more favorably hydrated compared to the positive ions. This remaining asymmetry must originate from structural differences in the hydration of fully charged positive and negative ions. Such differences are expected to diminish with increasing ion size as seen from the convergence in Fig. 3. The structural differences in the hydration of positive and negative ions have been presented previously;[17,57] here we summarize the key differences and discuss semiempirical means to account for their contribution to the hydration thermodynamics.

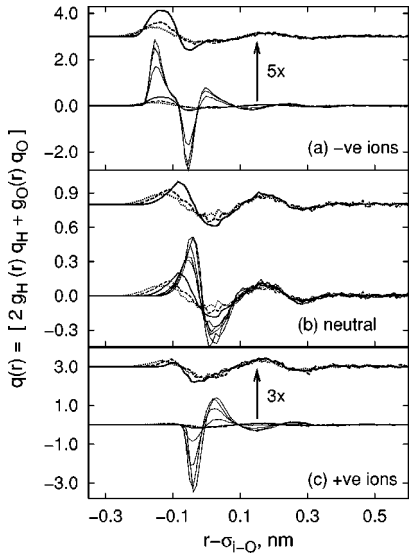

FIG. 5. Polarization charge density distribution around solutes of different sizes. Negative ions [panel (a)], the curves for the large solutes (0.6 nm, 0.8 nm, 1.0 nm) have been magnified by five and shifted vertically. Neutral solutes [panel (b)], the curves for the three large solutes are shifted vertically and replotted without magnification. Positive ions [panel (c)], the curves for the large solutes have been magnified by three and shifted vertically.

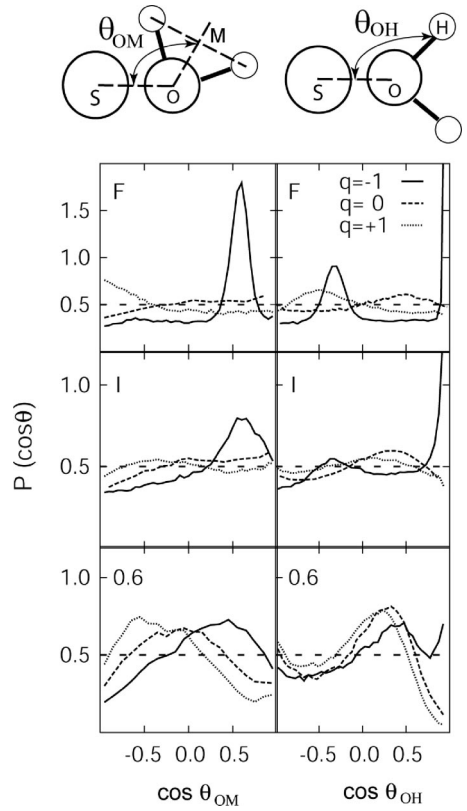

FIG. 6. Probability distribution of cosines of the angles, θ_{OM} and θ_{OH}, made by the oxygen–solute vector with the water dipole vector OM (left) and with the water OH bond vector (right), respectively. The label on the top left corner of each panel (F, I or 0.6) indicates the solute for which the curves are reported. Curves for negative (solid), neutral (dashed), and positive (dotted) solutes are shown.

B. Differences in structural hydration of positive and negative ions as a function of ion size

Figures 4–7 show ion–water radial distribution functions (rdf), polarization charge densities surrounding the ions, and orientational preferences of the water molecules hydrating the ions as a function of ion size. Collectively, these results capture the key differences between positive and negative ion hydration and the extent of their convergence for larger ions. Figures 4(a), 4(b), and 4(c) show ion–oxygen and ion–hydrogen rdfs for a fluoride ion in negative (F^-), neutral (F^0), and positive (F^+) charge states. Near the neutral F^0 solute, water structure shows the well-known features of hydrophobic hydration;[58] *viz.*, the first peaks of oxygen and hydrogen densities are approximately at the same location ($r \approx 0.35$ nm), indicating orientations of the HOH plane of water molecule almost tangential to the surface of the solute. At shorter separations, a tail of hydrogen density is also observed near F^0 solute. Thus, on average, water hy-

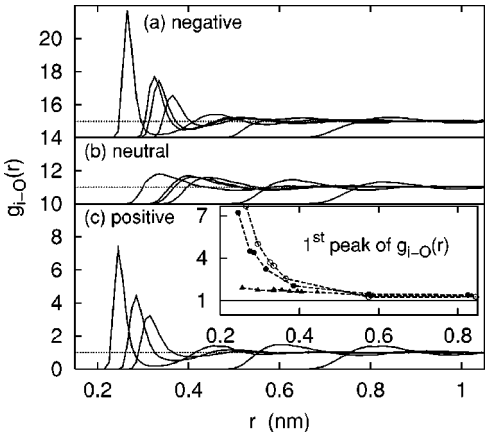

FIG. 7. Solute–oxygen radial distribution functions for all solutes listed in Table I in negative [panel (a)], neutral [panel (b)], and positive [panel (c)], charge states. The inset in the panel (c) shows the magnitude of the first peak in the solute–water oxygen rdf as a function of solute size. Increasing solute size leads to dewetting of the solute surface (see Ref. 25).

drogens are slightly closer to the solute center compared to oxygens, which leads to the small positive electrostatic potential at the center of the neutral solute. The proximity of hydrogens to solute center is also reflected in the polarization charge density profile, $(q_O g_{i-O}(r)+2q_h g_{i-h}(r))$, which shows a positive first peak (Fig. 5) for neutral solutes.

Charging the neutral F^0 solute in the negative or positive directions changes packing and orientational preferences in the first shell significantly. Favorable electrostatic interactions between the ion and water pull the water molecules closer toward the ion leading to significantly higher local density of water in the first hydration shell. The separation between the first peaks of ion–oxygen and hydrogen rdfs, seen in Fig. 4, provides information about the dominating water orientations in the first hydration shell. For example, near the F^- ion, the hydrogen peak is closer to the ion center compared to the oxygen peak by about 1 Å, equal to the OH bond length. That is, water molecules in the first hydration shell point one of their OH bond vectors directly toward the ion, and as a result the water dipole vector is not aligned in the radial direction. In contrast, near positive ions, the first oxygen peak is closer than the first hydrogen peak by about 0.6 Å indicating that on average the dipole vector is along the radial direction. This important difference is also clearly seen in cos θ distributions of angles θ_{OM} and θ_{OH} made by the OM (dipole) and OH vectors, respectively, with the oxygen–solute vector (as shown in Fig. 6). It appears that pointing one of the hydrogen atoms of the water molecule directly at the negative ion is, overall, energetically favorable as reflected in the magnitude of electrostatic potential induced at the center of F^- reported in Table II, which is about 20% higher than that at the center of F^+. In addition, thermal fluctuations of charge densities near negative ions also lead to a larger variance of that electrostatic potential compared to those measured at the center of positive ions.

Figures 4(d), 4(e), and 4(f) show similar rdfs for a larger ion ($\sigma_{i-O}=0.6$ nm) in the $-1e$, $0e$ and $+1e$ charge states. For notational simplicity, we denote these ions as 0.6^-, 0.6^0, and 0.6^+, respectively. Near the neutral 0.6^0 solute, features of oxygen and hydrogen rdfs appear similar to those near smaller neutral solutes, except that a weak dewetting is observed as indicated by the smaller value of the first peak height. The tail of hydrogen density at shorter separations persists, however, leading to a small positive potential at the solute center. Charging the neutral solute to the negatively charged 0.6^- solute enhances this tail in hydrogen density. However, the effect of the electric field of this larger ion on water molecules in the first hydration shell is much weaker than that observed for smaller negative ions. Indeed, the orientational preferences of hydration shell waters are only slightly different from those near the neutral solute as seen in Fig. 6. As stated above, the hydration structure near neutral solutes is slightly biased toward charging in the negative direction. In contrast, charging in the positive direction requires overcoming this unfavorable orientational bias before the vicinal water molecules can be aligned with the radial field of the positive ion. The effect of 0.6^+ on its hydration shell water molecules is so weak that it can not completely overcome this bias. As a result, a slight inward tail of hydrogen density persists near 0.6^+ leading to a small positive charge density near the ion as seen in Fig. 5. Orientational polarization preferences near 0.6^+ appear quite similar to its neutral counterpart (see Fig. 6).

The dewetting of nonpolar solutes with increasing solute size has been discussed in detail previously.[24–26,59] Water molecules hydrating small neutral solutes straddle the solute surface thereby maintaining favorable water–water interactions while simultaneously accommodating the small solute. With increasing solute size, however, water molecules in the vicinity lose interactions with nearby water molecules. This effect was characterized by Hummer and Garde in terms of a ''cavity expulsion'' potential in solute–water potential of mean force.[24] Similar ideas apply when considering the hydration of larger ions. With increasing ion size, the effect of the electric field of the ion on the vicinal water weakens leading to the dewetting of the solute surface (see Fig. 7), and to an approximate convergence of hydration structure (packing and orientations) to hydrophobiclike hydration for the large ions ($r \geqslant 0.5$ nm) studied here.

C. Empirical shifting of free energy

The above discussion identifies the origin of the asymmetry of hydration of positive and negative ions that remains after accounting for the asymmetry arising from the positive potential at the center of a neutral solute (Fig. 2). Specifically, this asymmetry arises from differences in the hydration structures near fully charged positive and negative ions. It is not possible to capture quantitatively the effect of these differences on the asymmetry in free energy in a straightforward manner. Several decades ago, Latimer, Pitzer, and Slansky (LPS)[8] suggested that the experimentally observed asymmetry in the hydration thermodynamics of simple monovalent ions (alkali and halides) can be empirically accounted for by simply shifting the crystal radii of positive and negative ions by constant magnitudes of 0.1 Å and 0.85 Å, respectively. Since LPS analyzed the hydration free energy for monovalent cation–anion pairs, the δG term presumably cancels out for each pair considered in that study.

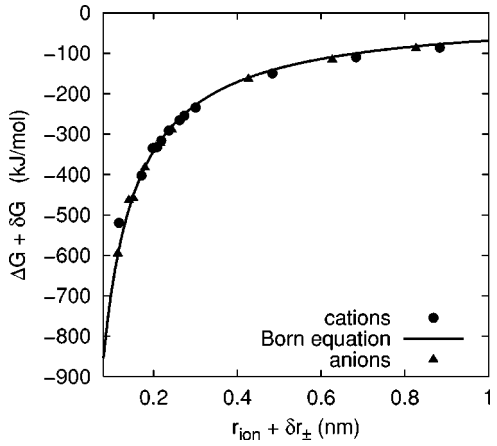

FIG. 8. The modified free energy of charging, $\Delta G+\delta G$, of ions plotted as a function of the modified ion radius $\sigma_{i-i}/2+\delta r_{\pm}$.

The ion–radii corrections that LPS suggested therefore must account for the residual asymmetry due to the structural differences.

Throughout this paper, we have plotted free energy of hydration as a function of ion radius defined here as $\sigma_{i-i}/2$, although reasonable alternative definitions of ion size will work equally well (Ref. 70) (e.g., van der Waals radius, or σ_{i-O}, etc.).[60–63] Following LPS, therefore, we write $r_{\mathrm{Born}}=r_{\mathrm{ion}}+\delta r_{\pm}$, where δr_{+} and δr_{-} are empirical shifts for positive and negative ion radii, respectively, that account for the hydration structural asymmetry described above. Such an empirical scheme would be useful only if the shifts δr_{+} and δr_{-} are constants, independent of the ion size. In that case, $|\delta r_{+}-\delta r_{-}|$, can be thought of roughly as the difference in the Born radii of positively and negatively charged states of the same ion and that its calculation will need to be done only for one ion. Within statistical uncertainties of the calculated free energy values, we find that $\delta r_{+}\approx 0.42$ Å and $\delta r_{-}\approx -0.15$ Å. Free energies of positive and negative ions plotted as a function of $[r_{\mathrm{ion}}+\delta r_{\pm}]$ show excellent agreement with the predictions of continuum model (Fig. 8). For the model LJ ions considered here, $|\delta r_{+}-\delta r_{-}|=0.57$ Å, practically independent of the ion size. That is the modified free energy of hydration of a positive ion of radius r and a negative ion of radius $r+0.57$ Å are identical. We note that applying shifts $\delta r_{\pm}$ without applying the initial modification, δG, does not lead to convergence in free energies over the entire ion size range, indicating the importance of both the terms. Therefore, we conclude that the shift from the positive potential at the center of a neutral solute, $\delta G=-q\langle\phi\rangle_0$, and the shift in ion radii, $\delta r_{\pm}$, accounting for the asymmetry in the structural hydration of fully charged ions, together account completely for the observed hydration asymmetry of positive and negative ions.

D. Water model dependence of ion hydration asymmetry

The structural and thermodynamic aspects of ion hydration, and specifically, their asymmetry with respect to the sign of ion charge will depend on the details of intermolecular interactions used in molecular simulations. We represented ions as simple Lennard-Jones solutes with the charge placed at the center of the ion, and water molecule using the three-point-charge SPC model. To obtain quantitative agreement with experimental data, one would need to parametrize ion–water potentials. For example, the repulsive part of the LJ potential is rather steep and softer repulsions may provide a more realistic representation of ions. In addition, the choice of water model (polarizable vs nonpolarizable, three point vs four or five point model) will affect the details of structure and thermodynamics.

Our goal here is not to develop potentials to better represent experimental data but to gauge the sensitivity of the observed asymmetry of hydration to the choice of water model employed. To this end, we performed calculations of the free energies of charging a fluoride ion in three additional nonpolarizable point charge models–SPC/E, TIP3P, and TIP4P (see Table III). Table IV lists the values of free energies of charging a fluoride solute from $0e$ to $\pm 1e$ charge states. We find that the asymmetry of hydration, quantified by $\Delta G_{F^+}-\Delta G_{F^-}$, is similar in SPC and SPC/E models, smaller by $\sim$30 kJ/mol in the TIP3P model, and higher by $\sim$30 kJ/mol in the TIP4P model of water. The partial charges on the oxygen and hydrogen sites of SPC/E water are only slightly higher in magnitude than that in SPC water. As a result, the hydration free energies of both positive and negative ions are slightly more favorable in SPC/E water. Interestingly, however, the hydration of F^+ ion is somewhat more favorable and that of F^- ion is less favorable by about 10 kJ/mol in TIP3P water. The electrostatic potential at the center of a neutral fluoride solute is nearly identical in SPC, SPC/E, and TIP3P water and does not account for differences in the hydration free energies in SPC or SPC/E and TIP3P models. Clearly, small differences in the LJ parameters, the HOH bond angle and the OH bond length, and the magnitude of partial charges are responsible for these subtle differences. On the other hand, for the TIP4P model, the negative charge

TABLE III. Parameters used to describe four different water models. σ_{O-O} and ϵ_{O-O} are the LJ parameters for interaction between oxygens, and q_H and q_O are the partial charges on hydrogen and oxygen sites, respectively. In the TIP4P water model, the partial negative charge, q_O is located 0.15 Å from the oxygen site along the H–O–H angle bisector.

Model	σ_{O-O}, nm	ϵ_{O-O}, kJ/mol	q_O, e	q_H, e	θ_{HOH}, deg	r_{OH}, nm
SPC	0.3169	0.6502	−0.8200	0.4100	109.47	1.0000
SPC/E	0.3169	0.6502	−0.8476	0.4238	109.47	1.0000
TIP3P	0.3151	0.6364	−0.8340	0.4170	104.47	0.9572
TIP4P	0.3154	0.6480	−1.0400	0.5200	104.52	0.9572

TABLE IV. The free energy of charging F^0 to F^- and F^+ charge states in four different water models calculated from MD simulations. The electrostatic potential at the center of the neutral F^0 solute and the difference between the hydration free energies of F^+ and F^- ions, are also reported in kJ/mol.

Water model	$e\langle\phi\rangle_0$	ΔG_{F^+}	ΔG_{F^-}	$\Delta G_{F^+}-\Delta G_{F^-}$
SPC	36.788	−297.0	−523.2	226.2
SPC/E	35.995	−298.0	−527.8	229.6
TIP3P	36.143	−308.1	−509.2	201.1
TIP4P	46.115	−290.5	−549.5	259.0

site is located off the oxygen center, 0.15 Å along the angle bisector OM. In addition, magnitudes of the partial charges in the TIP4P model are significantly higher. This results in a larger value of $\langle\phi\rangle_0$ in the TIP4P model and leads to the larger asymmetry of hydration compared to that in the three-point models as seen in Table IV. While the asymmetry of ion hydration is experimentally observed and is not simply the result of the choice of water model, these results emphasize that the extent of asymmetry depends sensitively on the geometric placement of partial charges in point charge models as well as subtly on the other details of intermolecular potentials.

IV. CONCLUSIONS

We have presented calculations of the free energy of charging neutral solutes to positive and negative charge states over a wide range of ion sizes in simple point charge model of water. These calculations clearly demonstrate the asymmetry of hydration of positive and negative ions. Specifically, for the same ion size the free energy of hydration is more favorable for negative ions compared to positive ions. While the aspects of asymmetry of ion hydration have been discussed previously, the range of solute sizes studied here is broad and, therefore, covers a wider range of ion charge density. The asymmetry of hydration arises primarily due to the asymmetry of charge distribution in the water molecule itself. That asymmetric charge distribution is reflected in (i) a small positive electrostatic potential at the center of a neutral solute, and (ii) clear structural (packing and orientational) differences in the hydration shells of the positive and negative ions. The asymmetry arising from the positive potential can be accounted for relatively easily as shown in Sec. III A. However, quantitative estimation of the asymmetry arising from the structural differences is difficult. We used the empirical shift of ion size to calculate the Born radius as suggested by Latimer, Pitzer, and Slansky[8] to account for the hydration structural asymmetry of the fully charged states. While that shift is empirical, it is ion size independent, and therefore useful. Together, these two contributions account completely for the asymmetry in the hydration of positive and negative ions over the entire range of ion sizes studied here.

We also explored the asymmetry of ion hydration in four commonly employed models of water. These nonpolarizable water models are rather similar to each other. Nevertheless, the calculated free energy of hydration and its asymmetry are sensitive to details of the placement of partial charges within the water molecule. The asymmetry of hydration of ionic solutes also in turn determines the ion association preferences as reflected in Volcano relationships[5] and are one of the important contributors to biomolecular interactions in solution. In light of the aforementioned results, studies of ion hydration thermodynamics and structure, and quantification of the hydration asymmetry of positive and negative ions could serve as a sensitive test of the utility of newly developed water models and ion–water interaction potentials that are applied in biological contexts.

ACKNOWLEDGMENTS

S.G. gratefully acknowledges partial financial support of ACS–PRF, NSF (CAREER award CTS-0134023), and NSF Nanoscale Science and Engineering Center for Directed Assembly of Nanostructures (DMR-0117792).

[1] P. H. Yancey, M. E. Clark, S. C. Hand, R. D. Bowlus, and G. N. Somero, Science **217**, 1214 (1982).
[2] K. D. Collins and M. W. Washabaugh, Q. Rev. Biophys. **4**, 323 (1985).
[3] V. A. Parsegian, Nature (London) **378**, 335 (1995).
[4] R. L. Baldwin, Biophys. J. **71**, 2056 (1996).
[5] K. D. Collins, Biophys. J. **72**, 65 (1997).
[6] M. G. Cacace, E. M. Landau, and J. J. Ramsden, Q. Rev. Biophys. **30**, 241 (1997).
[7] A. Kalra, N. Tugcu, S. M. Cramer, and S. Garde, J. Phys. Chem. **105**, 6380 (2001).
[8] W. M. Latimer, K. S. Pitzer, and C. M. Slansky, J. Chem. Phys. **7**, 108 (1939).
[9] H. L. Friedman and C. V. Krishnan, *Water-A Comperehensive Treatise*, Vol. 3 (Plenum, New York, 1973).
[10] Y. Marcus, *Ion Solvation* (Wiley, New York, 1985).
[11] G. Hummer, L. R. Pratt, and A. E. García, J. Phys. Chem. **100**, 1206 (1996).
[12] S. W. de Leeuw, J. W. Perram, and E. R. Smith, Proc. R. Soc. London, Ser. A **373**, 27 (1980).
[13] B. Jayaram, R. Fine, K. Sharp, and B. Honig, J. Phys. Chem. **93**, 4320 (1989).
[14] F. Figueirido, G. S. del Buono, and R. M. Levy, J. Chem. Phys. **103**, 6133 (1995).
[15] G. Hummer, L. R. Pratt, and A. E. García, J. Phys. Chem. **102**, 7885 (1998).
[16] G. Hummer, L. R. Pratt, and A. E. García, J. Chem. Phys. **107**, 9275 (1997).
[17] S. Garde, G. Hummer, and M. E. Paulaitis, J. Chem. Phys. **108**, 1552 (1998).
[18] G. Markovich, S. Pollack, R. Giniger, and O. Cheshnovsky, J. Chem. Phys. **101**, 9344 (1994).
[19] J. V. Coe, Int. Rev. Phys. Chem. **20**, 33 (2001).
[20] D. Asthagiri, L. R. Pratt, and H. S. Ashbaugh, J. Chem. Phys. **119**, 2702 (2003).
[21] H. S. Ashbaugh, J. Phys. Chem. **104**, 7235 (2000).
[22] G. Hummer, L. R. Pratt, A. E. García, S. Garde, B. J. Berne, and S. W. Rick, J. Phys. Chem. B **102**, 3841 (1998).
[23] H. S. Ashbaugh, S. Sakane, and R. H. Wood, J. Phys. Chem. B **102**, 3844 (1998).
[24] G. Hummer and S. Garde, Phys. Rev. Lett. **80**, 4193 (1998).

[25] F. H. Stillinger, J. Solution Chem. **2**, 141 (1973).
[26] K. A. Lum, D. Chandler, and J. D. Weeks, J. Phys. Chem. B **103**, 4570 (1999).
[27] H. J. C. Berendsen and D. van der Spoel, Comput. Phys. Commun. **91**, 43 (1995).
[28] E. Lindahl, B. Hess, and D. van der Spoel, J. Mol. Model. [Electronic Publication] **7**, 306 (2001).
[29] H. J. C. Berendsen, W. F. van Gunsteren, J. P. M. Postma, and J. Hermans, in Intermolecular forces: Proceedings of the 14th Jerusalem Symposium on quantum chemistry and biochemistry, edited by B. Pullman, 1981.
[30] S. Yoo, Y. A. Lei, and X. C. Zeng, J. Chem. Phys. **119**, 6083 (2003).
[31] D. E. Smith and L. X. Dang, J. Chem. Phys. **100**, 3757 (1994).
[32] S. J. Stuart and B. J. Berne, J. Phys. Chem. A **103**, 10300 (1999).
[33] P. Jungwirth and D. J. Tobias, J. Phys. Chem. B **106**, 6361 (2002).
[34] H. J. C. Berendsen, J. R. Grigera, and T. P. Straatsma, J. Phys. Chem. **91**, 6269 (1987).
[35] W. L. Jorgensen, J. Chandrasekhar, J. D. Madura, R. W. Impey, and M. L. Klein, J. Chem. Phys. **79**, 926 (1983).
[36] T. Darden, D. York, and L. Pedersen, J. Chem. Phys. **98**, 10089 (1993).
[37] S. Nose, Mol. Phys. **52**, 255 (1984).
[38] W. G. Hoover, Phys. Rev. A **31**, 1695 (1985).
[39] M. Parrinello and A. Rahman, J. Appl. Phys. **52**, 7182 (1981).
[40] S. Nose and M. L. Klein, Mol. Phys. **50**, 1055 (1983).
[41] S. Miyamoto and P. A. Kollman, J. Comput. Chem. **13**, 952 (1992).
[42] R. W. Zwanzig, J. Chem. Phys. **22**, 1420 (1954).
[43] G. Hummer and A. Szabo, J. Chem. Phys. **105**, 2004 (1996).
[44] B. Guillot and Y. Guissani, J. Phys. Chem. **99**, 8075 (1993).
[45] S. Garde, G. Hummer, A. E. García, L. R. Pratt, and M. E. Paulaitis, Phys. Rev. E **53**, R4310 (1996).
[46] S. Garde, A. E. García, L. R. Pratt, and G. Hummer, Biophys. Chem. **78**, 21 (1999).
[47] L. R. Pratt and A. Pohorille, Chem. Rev. (Washington, D.C.) **102**, 2671 (2002).
[48] G. Hummer, L. R. Pratt, and A. E. García, J. Phys. Chem. **99**, 14188 (1995).
[49] C. Y. Lee, J. A. McCammon, and P. J. Rossky, J. Chem. Phys. **80**, 4448 (1984).
[50] L. R. Pratt, J. Phys. Chem. **96**, 25 (1992).
[51] J. Alejandre, D. J. Tildesley, and G. A. Chapela, J. Chem. Phys. **102**, 4574 (1995).
[52] V. P. Sokhan and D. J. Tildesley, Mol. Phys. **92**, 625 (1997).
[53] H. S. Ashbaugh, Mol. Phys. **97**, 433 (1999).
[54] H. Patel, E. B. Nauman, and S. Garde, J. Chem. Phys. **119**, 9199 (2003).
[55] M. Paluch, Adv. Colloid Interface Sci. **84**, 27 (2000).
[56] Y. Marcus, J. Chem. Soc., Faraday Trans. **87**, 2995 (1991).
[57] L. R. Pratt and G. Hummer, *Computational Chemistry, Biophysics, and Aqueous Solutions: Simulation and Theory of Electrostatic Interactions in Solution* (AIP Conference Proceedings 492, Santa Fe, New Mexico, 1999).
[58] L. R. Pratt, Annu. Rev. Phys. Chem. **53**, 409 (2002).
[59] H. S. Ashbaugh and M. E. Paulaitis, J. Am. Chem. Soc. **123**, 10721 (2001).
[60] R. M. J. Noyes, Z. Phys. **84**, 513 (1962).
[61] R. H. Stokes, J. Am. Chem. Soc. **86**, 979 (1964).
[62] A. A. Rashin and K. S. Honig, J. Phys. Chem. **89**, 5588 (1985).
[63] J. K. Hyun and T. Ichiye, J. Phys. Chem. B **101**, 3596 (1997).
[64] L. X. Dang, J. Chem. Phys. **96**, 6970 (1992).
[65] L. X. Dang, J. Am. Chem. Soc. **117**, 6954 (1995).
[66] S. Koneshan, J. C. Rasaiah, R. M. Lynden-Bell, and S. H. Lee, J. Phys. Chem. **102**, 4193 (1998).
[67] D. van der Spoel, P. J. van Maaren, and H. J. C. Berendsen, J. Chem. Phys. **108**, 10220 (1998).
[68] Although we have chosen to represent the ion size by $r_{\text{ion}}=\sigma_{\text{ion–ion}}/2$, other reasonable choices of ion size do not alter the analysis and conclusions that follow.
[69] We do not refer to $q\langle\phi\rangle_0$ term as a ''correction'' term, because technically no ''correction'' needs to be made to the ΔG values. Our goal here is simply to identify the origins of hydration asymmetry and quantify them.
[70] The shift due to positive electrostatic potential does not rely explicitly on the choice of the parameter used to represent the ion size, but depends on the measured values of cumulants.